Energy Attenuation Prediction of Dye-Doped PMMA Microfibers by Backpropagation Neural Network

Hang Yu, Juan Liu ⬤, Jinjin Han, Minghui Chen, Mingjun Ke, Zhili Lin ⬤, *Senior Member, IEEE*, Zhijun Wu ⬤, Jixiong Pu ⬤, *Member, IEEE*, Xining Zhang ⬤, and Hao Dai ⬤

Abstract—To figure out the energy attenuation of micro/nanofibers (MNFs) more flexibly and conveniently, a backpropagation neural network (BPNN) is proposed to forecast the output intensity of rhodamine B (RhB) doped polymer microfibers (PMFs). According to the diameter, doping concentration, and propagation distance (*L*), we realize the *L*-dependence of output energy predictions for the excitation light (I_E) and fluorescence (I_F) of the doped PMFs. Hundreds of propagation distance-intensity data pairs acquired from dozens of RhB doped PMFs are used for the BPNN training. The prediction ability of the model is evaluated by the root-mean-square error (RMSE), the mean absolute percentage error (MAPE), and R^2. The output intensity prediction performance of BPNN is compared with the traditional exponential-fitting (EF) method. The prediction results indicate that the two-hidden-layer network with one and seventeen neurons respectively provides the best performance. After training, BPNN gives a good intensity prediction for both the I_E (RMSE = 3.16×10^{-2}, MAPE = 7.3%, and $R^2 = 0.9802$) and the I_F (RMSE = 0.91×10^{-2}, MAPE = 0.89%, and $R^2 = 0.9696$) from the output end of the PMF with different diameters and doping concentrations. The energy losses of the two kinds of light from different doped PMFs are also calculated based on the predicted values, which are similar to the ones obtained from the EF method. The approach based on the BPNN prediction for the energy attenuation of the PMFs shows superiority in flexibility and applicability toward the traditional methods, which could promote the optimal design of the MNF devices and the practical application.

Index Terms—Backpropagation neural network, dye-doped polymer microfiber, energy attenuation prediction.

Hang Yu, Juan Liu, Jinjin Han, Minghui Chen, Mingjun Ke, Zhili Lin, Zhijun Wu, Jixiong Pu, and Xining Zhang are with the Fujian Key Laboratory of Light Propagation and Transformation, College of Information Science and Engineering, Huaqiao University, Xiamen 361021, China (e-mail: yuhanghqu@163.com; liujuanhqu@163.com; hjj1787703153@163.com; 905327317@qq.com; 362214335@qq.com; zllin2008@gmail.com; zhijunwu@hqu.edu.cn; jixiong@hqu.edu.cn; zhangxn_hqu@163.com).

Hao Dai is with the Institute of Ocean Exploration Technology, College of Ocean and Earth Sciences, Xiamen University, Xiamen 361005, China (e-mail: daihaozxn@163.com).

I. INTRODUCTION

FUNCTIONALIZED polymer micro/nanofibers (PMNFs), which are doped with dye molecular [1], [2], metal nanoparticles [3], [4], quantum dots [5], [6], and so on, is a kind of versatile building block for constructing photonic circuits and components [7]–[9]. As the energy loss of PMNF is one of the important factors affecting the propagation and conversion of light [10], the intensive study for the attenuation is the basis for the photonic devices based on doped PMNFs.

Typically, there are two common ways to obtain the energy attenuation of micro/nanofibers, which are theoretical calculation and experimental measurement. However, due to the uncertainty of the doped PMNF's refractive index and the complex structure of the PMNF device, the calculated loss is usually different from the actual value. The direct measurement for the decaying energy in the micro/nanofiber by experiments often relies on multiple measurements for one certain micro/nanofiber [11]–[13]. Generally, a straight optical waveguiding suffers the energy loss mainly caused by the waveguiding of the light [11], the diameter of the micro/nanofiber [14], the doping concentration [13] and its agent [15]. The experiments are carried out on the micro/nanofiber with a fixed diameter and doping concentration, and the result is difficult to quantitatively extend to the waveguidings with other diameters or doping concentrations. Consequently, both the theoretical and experimental methods fail to flexibly and quickly obtain the energy attenuation of PMNF with arbitrary doping concentration and diameter. However, as the basic unit for building active optical microdevices, flexible and accurate prediction of microfiber energy loss is crucial for the optimal design based on doped PMNFs devices in practical, such as light-emitting devices in micro/nano scale [15] and microlasers [16]. Recently, the artificial neural network has been employed for predicting the adsorption effect of nanoparticles on water pollutants [17]–[21], which shows that it is possible to evaluate the energy attenuation of functionalized PMNFs by self-learning techniques.

Therefore, to efficiently provide the energy attenuation of doped polymer microfibers (PMFs), we use a backpropagation neural network (BPNN), which has learned from a large amount of optical experiment data, to predict the energy attenuation of rhodamine B (RhB) doped PMFs based on its doping concentration and diameter. Under an optical microscope, we measured around 500 normalized light intensity-propagation distance data pairs from ~50 RhB-doped PMFs from the optical

experiments. These data are taken as the data set for BPNN training and prediction. In the BPNN, the wavelengths, doping concentrations, diameters of PMF, and propagation distance are considered input neurons, while the excitation-light and fluorescent intensities at the output end of the PMF are used as the predictant variables. The well-trained BPNN is able to directly forecast the propagation-distance-dependence of energy attenuation in doped PMFs with different doping concentrations and diameters.

II. THEORY

A. Energy Loss Calculation

The energy propagating along a straight microfiber weakens quickly with the growth of the propagation distance (L) [1], [3], [22]. The attenuation of light intensity is affected by many factors, such as the incident wavelength [3], [23], [24], diameter [6], [25], [26], and doping concentration [13], [27]. As for the microfiber with a certain diameter, the energy loss of the incident light in the microfiber is described by the decaying exponential function as follows [11]:

$$I(L) = I_0 e^{-L/L_0} \tag{1}$$

in which $I(L)$ is the output intensity of the propagation distance L, I_0 is the initial input intensity. L_0 represents the propagation length, which is the distance that the output intensity of the microfiber decreases to I_0/e. We use the average energy loss rate (β) to describe the energy attenuation along with a certain propagation distance of a microfiber, which is defined as follows:

$$\beta = \frac{-10 \log_{10}(I_{L_2}/I_{L_1})}{L_2 - L_1} \tag{2}$$

where I_{L_1} and I_{L_2} are the normalized output intensities corresponding to L_1 and L_2 respectively. The propagation length-intensity data pairs of the microfiber could be measured in the experiments and the energy decaying trend could be further analyzed by fitting the intensity according to (1). This approach is suitable for microfibers with experimental data in advance, which is a traditional exponential-fitting method.

B. BPNN Analysis

Generally, the input variables of a neural network are the key factors that affect the output variables. By the learning of a large amount of experimental data, the network, which establishes the input-output mapping relationship, could realize the output prediction under different input variables.

As a classical neural network, the topological diagram of BPNN used in this paper is shown in Fig. 1. The normalized output intensity (I_N) of an RhB-doped PMF, which is the predicted aim, is the only variable in the output layer. The input layer has four neurons, which are the propagation distance (L), microfiber diameter (d), doping concentration (c), and the incident wavelength/wavelengths (λ). These four variables are the main influences on the energy loss in the microfiber. Among them, λ is used to distinguish whether the output intensity is the intensity of excitation light or the fluorescence. The hidden layer is located between the input and output layers, and the numbers
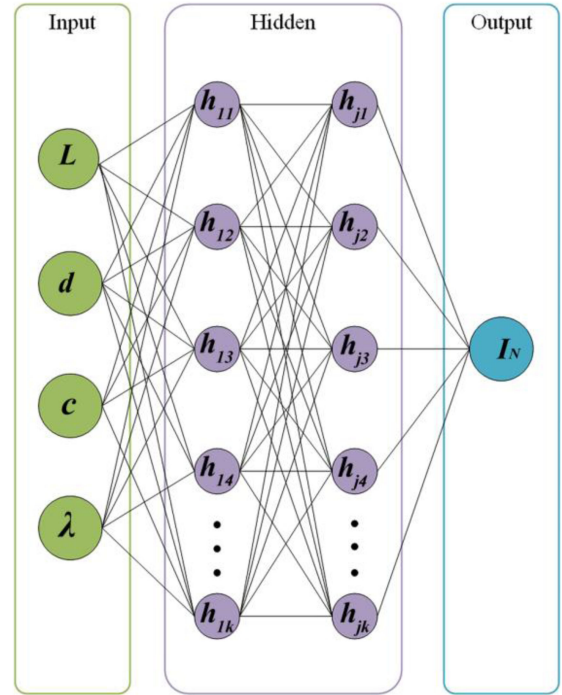
Fig. 1. Topological structure of the BPNN used to predict the normalized intensity of the dye-doped PMF. The neuron in the hidden layer is represented as h_{jk} [28].

of layers and neurons can be adjusted according to the prediction effect of the network.

The performance of the BPNN is evaluated by comparing the predicted data to the corresponding measured ones. The root-mean-squared error (RMSE), mean absolute percentage error (MAPE), and coefficient of determination (R^2) are employed to compare the predicted performance of the BPNN, which are calculated by the following equations respectively [29]:

$$\text{RMSE} = \sqrt{\frac{1}{n} \sum_{i=1}^{n} (P_i - M_i)^2} \tag{3}$$

$$\text{MAPE} = \frac{1}{n} \sum_{i=1}^{n} \left| \frac{M_i - P_i}{M_i} \right| \tag{4}$$

and

$$R^2 = 1 - \frac{\sum_{i=1}^{n} (P_i - M_i)^2}{\sum_{i=1}^{n} (\overline{M} - M_i)^2} \tag{5}$$

where, M_i and P_i represent the measured and predicted values of normalized intensity, respectively. n is the number of L-I_N data pairs obtained from one RhB-doped PMF. $\overline{M}$ is the average value of all the measured data. The prediction result with smaller values of RMSE and MAPE and a larger value of R^2 (1 for the best), which means indicates a better-predicted skill of the BPNN [29], [30].

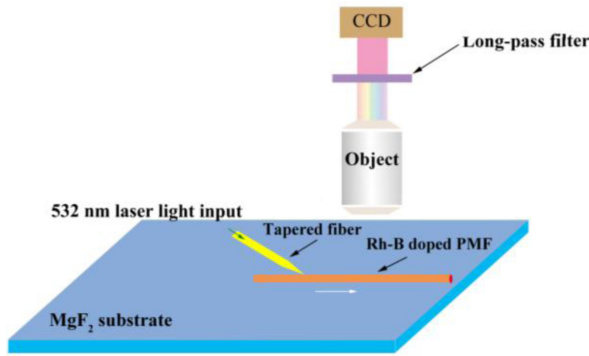Fig. 2. Schematic diagram of the experimental setup for energy measurement.

Fig. 3. Topical microimages of the energy measurement of an RhB-doped PMF. (a) Bright-field optical microimage of the tapered fiber coupling light into an RhB-doped PM with the light off. Typical optical microimage of fluorescent excitation in an RhB-doped PMF without (b) and with (c) the filter, respectively. The diameters of the PMF are 1.8 μm. The propagation distances are ~80 μm for all the images. Scale bars for all images are 20 μm.

III. EXPERIMENTS

A. Optical Experimental Setup

Fig. 2 shows the schematic diagram of the energy measurement of RhB-doped PMF by the waveguiding excitation method under an optical microscope [31]. The doped PMF deposited on a MgF$_2$ substrate is coupled to the tapered fiber which is fabricated from an optical fiber by the flame-heated drawing technique [25]. The light of 532-nm wavelength is launched by the tapered fiber for energy excitation. The length of the energy propagating along the doped PMF (L) could be adjusted by moving the tapered fiber along the PMF. The moving direction is indicated by the white arrow. The adjusting process could be monitored by a CCD mounted on an optical microscope. Meanwhile, the microimage of the excited PMF could also be captured for further calculation. By inserting the long-pass filter before the CCD, the intensity of RhB fluorescence from the PMF could be recorded by removing the excitation light.

Experimentally, we fabricated the RhB-doped PMF by the solution drawing method [32], [33]. The doped polymer solution is the chloroform solution with poly (methyl methacrylate) (PMMA) and RhB. The doping concentration (c) varies with the RhB quantity in the 750-mg PMMA, which is 2.0 mg/g, 2.4 mg/g, 2.8 mg/g and 3.0 mg/g, respectively.

The typical optical micro-image of the energy loss measurement is shown in Fig. 3. By the waveguiding excitation method which is mentioned in detail in [11], the RhB fluorescence in the doped 1.80-μm-diameter PMF is excited by the tapered fiber from the left. The propagation distance could be measured without light, which is 80 μm in Fig. 3(a). Fig. 3(b), which is the corresponding dark-field microimage of Fig. 3(a), shows the sufficient excitation of the fluorescence in the RhB-doped PMF. The saturated bright spot at the coupling point indicates the high coupling and excitation efficiencies in the experiment. With the fluorescence indication, we could observe the interference pattern along the doped PMF, which are usually recorded in the dye-doped microfibers excited by the waveguiding coupling approach [26]. When inserting the filter to avoid the wavelength before 590 nm, most RhB fluorescence emitted from the doped PMF travels oscillated and gradually faded along the PMF (Fig. 3(c)).
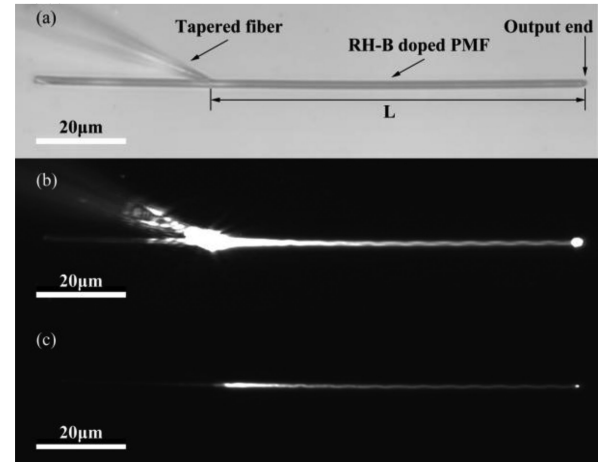
TABLE I
DIAMETER DISTRIBUTION OF RHB DOPED PMFs WITH DIFFERENT DOPING CONCENTRATIONS

c (mg/g)	d (μm)			
	Average	Standard deviation	Maxmum	Minimum
2.0	1.80	0.02	1.81	1.78
2.4	1.81	0.09	1.90	1.72
2.8	1.79	0.01	1.80	1.77
3.0	1.78	0.08	1.86	1.70

To acquire the output intensity of a doped PMF, we use the gray value of the output end to represent the output intensity of the PMF. As [11], [34] mentioned before, the 64×64-pixel area, which is corresponding to the output spot of the doped PMF, is firstly intercepted from the dark field images taken without and with the filter. The calculated gray values of the output spots in the corresponding images are considered as the total light (I_{total}) and fluorescent intensities (I_F). The normalized intensities, which are denoted as I_E and I_F, are corresponding to the output intensities of excitation light and fluorescence of the doped PMF respectively. I_E could be obtained by subtracting I_F from I_{total} in our study. We measured 509 groups of L-I_E data pairs from 52 RhB-doped PMFs and 431 groups of L-I_F data pairs from 45 doped PMFs in our work. The diameter distribution of RhB-doped PMFs with different c is listed in Table I.

B. Structure of the BPNN for Intensity Prediction of Doped PMFs

We randomly divided hundreds of data pairs into the training set and the testing set. The BPNN program is written and run on MATLAB software platform (R2017b, Version number 40640758). The BPNN which has learned from the training data set predicts the normalized output intensity (I_E and I_F) of the PMF at different L. The main structure and parameters of the BPNN are shown in Table II.

TABLE II
BPNN SETTING FOR ENERGY LOSS PREDICTION OF RHB DOPED PMMA MICROFIBERS

Model parameters & settings	Value/Name
Neurons in the input layer	L, d, c and λ
Neurons in the output layer	I_E or I_F
No. of hidden layers (neurons in each hidden layer)	2 (1, 17)
No. of training data pairs	443 for I_E, 365 for I_F
No. of testing data pairs	66 for I_E, 66 for I_F
Error goal	$1.0e^{-2}$
Training function	trainlm
Activation function for input-hidden layer	tansig
Epoch (Iteration number)	1000

Fig. 4. BPNN's predicted skill of the light attenuation in the 1.69-μm-diameter doped PMFs with the concentration of 3.0 mg/g. (a) The excitation light. (b) The fluorescent light.

Considering the different energy attenuation characteristics of the excitation light and the fluorescence in the doped PMF, we train the BPNN with different data pairs. That is, the network with L-I_E data pairs as the input parameter is used to predict the attenuation of the excitation light intensity (I_E), and the one with L-I_F is used to predict the decay of fluorescence (I_F). The predicting performance of the BPNN is evaluated by the RMSE, MAPE, and R^2 values, which are calculated by (3), (4), and (5). To obtain the optimal structure of BPNN, we compare the prediction results given by the networks with different numbers of neurons (1∼30) and hidden layers (1∼3). The prediction performances given by these BPNNs are evaluated by the above indexes (RMSE, MAPE, and R^2), which are listed in the Supplemental document (Table S1 for I_E and Table S2 for I_F). After comparing the results from dozens of BPNNs with different structures, the best intensity-prediction performance is obtained by the two-hidden-layer BPNN with one and seventeen neurons. Except for the difference in the input wavelength, the weight, and bias values (listed in Table S3 and Table S4), the BPNN which is used to predict I_E and I_F respectively has the same structures in the following predicting experiments.

IV. ANALYSIS AND DISCUSSION

A. Intensity Prediction of the BPNN

To predict the normalized intensity of the doped PMF by BPNN, the input variables for testing are $d = 1.69$ μm, $c = 3.0$ mg/g and L is in the range of 32∼153 μm with a step of ∼10 μm. The predicted results and the comparison with the corresponding measured values are shown in Fig. 4.

For both I_E and I_F, the predicted intensity by the BPNN (blue star) has a significant attenuation trend with the increase of L. When L is from ∼30 μm to ∼70 μm, the output energy decreases quickly. When L is larger than ∼100 μm, the output intensity of doped PMF tends to be stabilized.

For the excitation light in the doped PMF (Fig. 4(a)), the RMSE and MAPE of the predicted I_E are 3.16×10^{-2} and 7.30%, respectively. The value of R^2 is 0.9802. The high MAPE indicates the obvious disagreement between the measured (red circles) and predicted intensity values (blue stars) in the propagation distance from ∼50 μm to ∼90 μm. To compare the BPNN-predicted results to the traditional exponential-fitting method, we fitted the measured I_E according to (1). The fitting
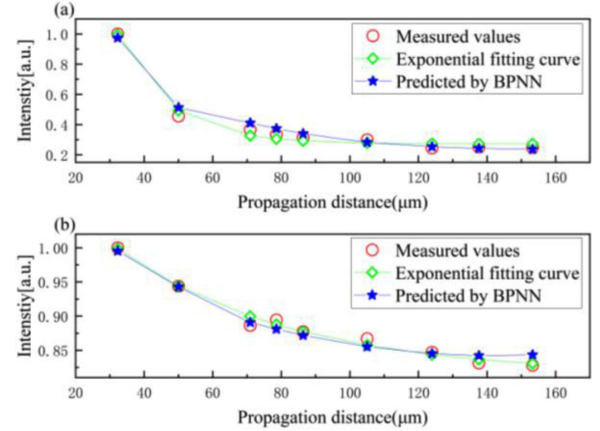
curve is close to the predicted I_E in Fig. 4(a). Moreover, the difference between the fitted values (green diamonds) and the experimental value is also calculated by RMSE, MAPE, and R^2 which are respectively 2.72×10^{-2} and 8.10%, and 0.9854. This indicates that the excitation energy attenuation predicted by the BPNN is similar to the exponential fitting of the experimental value.

Fig. 4(b) shows the prediction of the normalized fluorescence intensities which are the same position as the ones in Fig. 4(a). The fluorescence changing tendency predicted by the BPNN (blue stars) has a good agreement with the result of exponential fitting results (green diamonds). By comparing with the actual measured data (red circles), the RMSEs of the predicted values and fitting values are 0.91×10^{-2} v.s. 0.64×10^{-2} while MAPEs are 0.89% v.s. 0.54%, respectively. The R^2 values of the BPNN prediction and exponential fitting are 0.9696 and 0.9852, respectively.

Therefore, the BPNN we used here could effectively forecast the excitation light and fluorescent intensity attenuations of RhB-doped PMF. For their similar RMSE, MAPE, and R^2 values of the BPNN and exponential-fitting method, the BPNN could give a good prediction of the L-dependence of output energy, which has the same performance as the traditional method.

Besides, the attenuation amplitudes of I_E and I_F are different from each other. This could be attributed to their difference in the physical processes in the doped PMF. The excitation light is not only affected by the propagation loss in our experiments but also continuously excites the fluorescence in the waveguide which has to convert its energy. This is mainly due to the different physical processes of excitation light and fluorescence in the doped PMFs. When the fluorescence is propagating along the straight waveguide, it is only affected by the characteristics of the material and suffers the propagation loss which increases with the propagation length. As for the excitation light, it is not only affected by the propagation loss but also converts its energy when it continuously excites the fluorescence in the waveguide [13], [34].
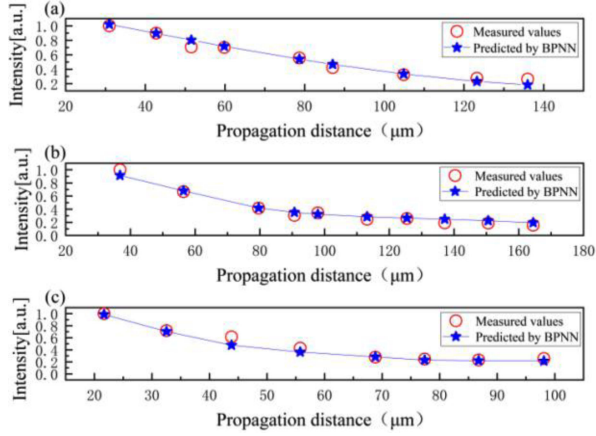
Fig. 5. BPNN prediction results of the measured L-I_E pairs obtained from the 3.0 mg/g-doping-concentration PMFs with different diameters. (a) $d = 1.74$ μm, (b) $d = 1.81$ μm, and (c) $d = 1.85$ μm.

TABLE III
BPNN-PREDICTION AND AVERAGE LOSS RATES OF I_E IN THE RhB DOPED PMFS WITH DIFFERENT DIAMETERS AND 3.0-MG/G CONCENTRATION

d (μm)	BPNN prediction			Average loss rate (β_E, 10^{-2} dB/μm)	
	RMSE (10-2)	MAPE (%)	R^2	$\beta_{E\text{-}P}$	$\beta_{E\text{-}M}$
1.74	4.78	9.03	0.9654	6.89	7.13
1.81	4.24	12.67	0.9715	6.63	7.56
1.85	5.69	8.77	0.9533	6.38	7.01

B. Generalization of the BPNN for the Doped PMFs With Different Diameters and the Same Concentration

The BPNN used to predict the output light intensity in this study has multiple input parameters, such as the diameter of the doped PFM and the doping concentration. Therefore, the well-trained BPNN with two hidden layers can directly predict the normalized output intensities of the PMFs with different diameters. We predicted three doped PMFs with the same doping concentration (3.0 mg/g) and different diameters (d are respectively 1.74 μm, 1.81 μm, and 1.85 μm), and analyzed the changes of I_E and I_F with L by the predicted values.

1) Excitation Intensities: The BPNN-forecasted I_E and I_F are compared with their corresponding experimental measured values, which are shown in Fig. 5 and Table III. The structure of the BPNN employed in Fig. 5 is the same as the one used in Fig. 4. For all the three PMFs, the decaying tendencies of the predicted I_E could be observed obviously in Fig. 5. Most of the predicted intensities are close to their corresponding measured values except for the ones of the 1.74-μm-diameter PMF in Fig. 5(a).

We calculated the RMSE, MAPE and R^2 values in Fig. 5(a), which are 4.78×10^{-2}, 9.03%, and 0.9654, respectively. The evaluation indexes show similar forecasted performance to the one in Fig. 4(a). Meanwhile, for the doped PMFs with diameters of 1.81 μm and 1.85 μm (Fig. 5(b) and (c)), the RMSEs of the two are $\sim 5 \times 10^{-2}$ and the MAPE values are around 10%. The values of R^2 are over 0.95. The details of the evaluation parameters are shown in Table III. The BPNN has good predictive performances for I_E of three doped PMFs with different diameters.
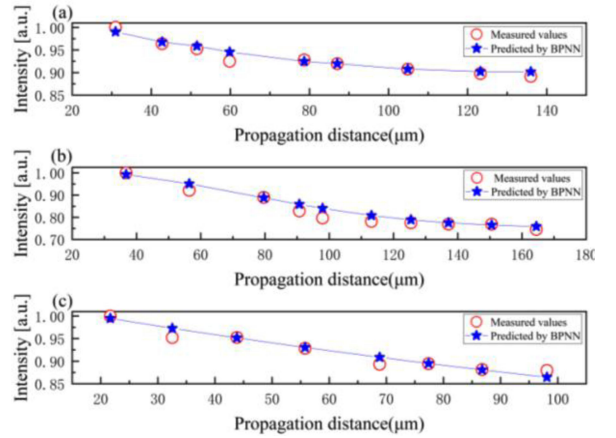

Fig. 6. Predicted I_F for the 3.0 mg/g-doping-concentration PMFs with different diameters. (a) $d = 1.74$ μm, (b) $d = 1.81$ μm, and (c) $d = 1.85$ μm.

Moreover, for the I_E obtained from the above PMFs, we compare their energy losses with the propagation distance from ~ 40 μm to ~ 100 μm, which are listed in Table III. According to (2), the average loss rates, which are calculated by the predicted and the measured values, are denoted by $\beta_{E\text{-}P}$ and $\beta_{E\text{-}M}$, respectively. $\beta_{E\text{-}P}$ and $\beta_{E\text{-}M}$ of each PMF in Table III are similar to each other. The average loss rates (β_E) are around 6.5×10^{-2} dB/μm. β_E in this study are in the ranges which are reported in [13] (The average losses are $\sim 8.3 \times 10^{-2}$ dB/μm for the 2.8 mg/g PMF and $\sim 6.3 \times 10^{-2}$ dB/μm for the 3.2 mg/g PMFs according to [13].) Although the doping concentrations are the same for all the three PMFs, β_E fails to show the obvious declining trend with the diameter increasing, which is always be found in the micro/nanowires [3]. This is mainly attributed to the reason that the loss in Table III reflects the property of a single waveguide and is lacks statistics on multiple wires.

2) Fluorescent Intensities: Using the same network structure, we predicted the I_F of the above three PMFs and analyze their energy changes. The predicted results and corresponding measured data are shown in Fig. 6. Although the diameters are different, the predicted I_F of the three PMFs are adjacent to the experimental values.

According to the RMSE and MAPE values listed in Table IV, the RMSE are all lower than 2.20×10^{-2} (0.89×10^{-2}, 2.20×10^{-2} and 1.08×10^{-2} in the order of diameter from small to large), and the values of MAPE are lower than 2.15% (0.70%, 2.14%, and 0.83% respectively). The R^2 values are higher than 0.92. It shows that the BPNN has a good predictive skill for I_F prediction for the doped PMFs with different diameters.

The prediction performances of I_F in Fig. 6 are much better than the ones of I_E (Fig. 5). This is because the fluorescence attenuation is simply caused by the characteristics of the material while the energy loss of the excitation light is more complicated, which should also consider the energy conversion [13].

Moreover, to evaluate the energy loss based on the BPNN prediction, we use the predicted values and experimental values to calculate the energy losses of I_F according to (2). The comparison is as shown in Table IV. For each PMF, although different values are used for the average loss rate calculations, $\beta_{F\text{-}P}$ is

TABLE IV
BPNN-PREDICTED SKILLS AND AVERAGE LOSS RATES OF IF IN THE RhB
DOPED PMFs WITH DIFFERENT DIAMETERS AND 3.0-MG/G CONCENTRATION

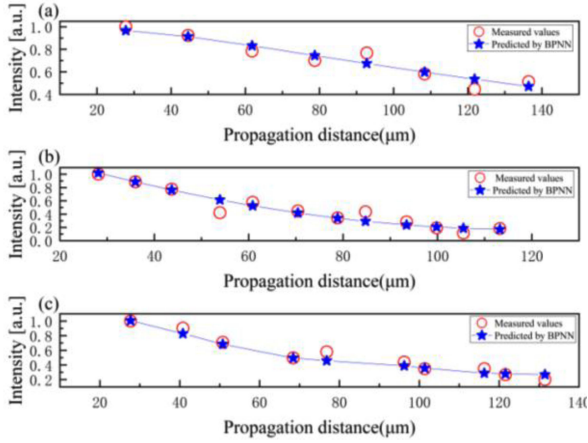| d (μm)	BPNN prediction			Average loss rate (β_F, 10^{-2} dB/μm)	
	RMSE (10^{-2})	MAPE (%)	R^2	$\beta_{F\text{-}P}$	$\beta_{F\text{-}M}$
1.74	0.89	0.70	0.9266	0.35	0.42
1.81	2.20	2.14	0.9217	1.18	1.61
1.85	1.08	0.83	0.9289	0.78	0.53

Fig. 7. BPNN prediction results of the measured L-I_E pairs obtained from the 1.8-μm-diameter PMFs with different concentrations. (a) c = 2.0 mg/g, (b) c = 2.4 mg/g, and (c) c = 2.8 mg/g.

TABLE V
PREDICTED SKILLS AND ENERGY LOSSES OF EXCITATION LIGHT IN
1.80-μM-DIAMETER DOPED PMFs WITH DIFFERENT DOPING
CONCENTRATIONS

c (mg/g)	BPNN prediction			Average loss rate (β_E, 10^{-2} dB/μm)		Loss rate (10^{-2} dB/μm)[13]
	RMSE (10^{-2})	MAPE (%)	R^2	$\beta_{E\text{-}P}$	$\beta_{E\text{-}M}$	
2.0	5.47	7.46	0.9091	2.89	3.15	3.5±1.5
2.4	7.61	16.22	0.9227	10.10	10.80	10.2±3.3
2.8	5.66	10.32	0.9505	6.05	6.82	6.3±4.5

closer to $\beta_{\text{F-M}}$ for the effective prediction of I_F by the BPNN. The average loss rate of the fluorescence ($\sim$1.0×10^{-2} dB/μm) is much lower than its corresponding one of the excitation light ($\sim$6.5×10^{-2} dB/μm in Table III).

C. Energy Prediction for RhB Doped PMFs With Different Concentrations and the Same Diameter

To further verify the generalization ability of the BPNN for the dye-doped PMFs, we predicted and analyzed the output intensities of three RhB-doped PMFs with different doping rates and the same diameters (d = 1.80 μm). Their doping concentrations are 2.0 mg/g, 2.4 mg/g, and 2.8 mg/g, respectively.

1) Excitation Intensity: The BPNN-predicted I_E and their corresponding measured values of the three PMFs are shown in Fig. 7. The predicted I_E of each PMF (blue stars) decays rapidly as L increases. Most of the predicted intensities are close to their corresponding measured values (red circles).

From the comparison of RMSE and MAPE in Table V, the RMSE values of the 2.0-mg/g and 2.8-mg/g-concentration PMFs
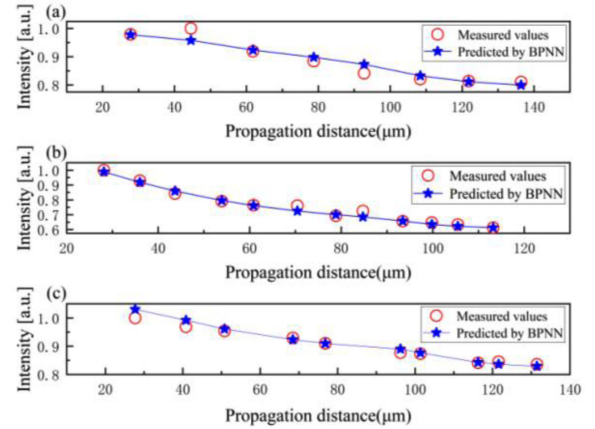

Fig. 8. Predicted I_F for the 1.8-μm-diameter PMFs with different concentrations. (a) c = 2.0 mg/g, (b) c = 2.4 mg/g, and (c) c = 2.8 mg/g.

are both less than 6.0×10^{-2}, and MAPEs are lower than 11% (7.46% v. s. 10.32%). The R^2 values are over 0.90. The largest deviation between the predicted values and the experimental values is obtained from the PMF with a doping concentration of 2.4 mg/g (RMSE = 7.61×10^{-2}; MAPE = $\sim$16%; R^2 = 0.9227). We attribute it to the disagreement of the forecasted and measured intensities at L = $\sim$54 μm and $\sim$85 μm, which increases the overall deviation. Despite several deviation data, the BPNN has good predictive and generalized abilities for the normalized I_E of PMFs with a diameter of 1.80 μm and different doping rates.

Table V also lists the energy losses of excitation light in these PMFs with different doing rates. $\beta_{\text{E-P}}$ is the average loss rate calculated by the prediction values while $\beta_{\text{E-M}}$ is the one by the measured values. When the propagation distance is growing from $\sim$40 μm to $\sim$100 μm, $\beta_{\text{E-P}}$ and $\beta_{\text{E-M}}$ of each PMF are close to each other. This is mainly because the BPNN can give a predicted I_E closer to the corresponding measured value. For each doped PMF, both $\beta_{\text{E-P}}$ and $\beta_{\text{E-M}}$ are in the loss range which has been reported in Ref. [13]. Comparing the average loss rates obtained by the predicted and measured values, the most serious energy loss of these three PMFs is acquired when the doping concentration is 2.4 mg/g ($\sim$10.1×10^{-2} dB/μm), which is mainly due to the consumption of higher excitation light energy for the excitation of fluorescence at this concentration [13].

2) Fluorescent Intensity: We also use the same BPNN to predict the I_F of the above three PMFs. Fig. 8 shows the L-dependence of the fluorescent intensities. The BPNN has the ability to forecast the declining trend of the normalized I_F with the growth of propagation distance. Compared with the fluorescence output measured by the experiment (red circle), except for some propagation distances (such as the data at L = $\sim$ 45 μm and $\sim$ 93 μm in Fig. 8(a), L = $\sim$ 70 μm and $\sim$ 85 μm in Fig. 8(b), and L = $\sim$28 μm and $\sim$41 μm in Fig. 8(c)), the predicted I_F (blue stars) are agree well with the corresponding measured values.

The RMSE and MAPE values, which evaluate the performance of the BPNN, are listed in Table VI. The RMSEs of

TABLE VI
PREDICTION EFFECT AND ENERGY LOSSES OF FLUORESCENCE IN THE
1.80-μM-DIAMETER DOPED PMFS WITH DIFFERENT DOPING
CONCENTRATIONS

c (mg/g)	BPNN prediction			Average loss rate (β_F, 10^{-2} dB/μm)		Loss rate (10^{-2} dB/μm) [13]
	RMSE (10^{-2})	MAPE (%)	R^2	$\beta_{F\text{-}P}$	$\beta_{F\text{-}M}$	
2.0	2.02	1.65	0.9181	0.95	1.34	1.8±0.5
2.4	1.79	1.74	0.9759	2.34	2.03	3.6±1.9
2.8	1.36	1.07	0.9393	0.88	0.74	1.8±0.9

the three are much lower than the ones of I_E shown in Table V, which are 2.02×10^{-2}, 1.79×10^{-2}, and 1.36×10^{-2}. The MAPEs are less than 1.8% (1.65%, 1.74%, and 1.07% respectively). The values of R^2 are higher than 0.91 (0.9181, 0.9759, and 0.9393, respectively). The I_F predicted results have lower values of RMSE and MAPE with higher R^2. This indicates that the difference between the predicted and measured values of I_F is smaller than that of I_E. Consequently, although the doping concentration is different, the BPNN with the same network structure as the one predicted I_E can achieve an accurate prediction of I_F.

Based on the prediction results of the BPNN and the actual data, the energy losses of I_F from $L = \sim 40$ μm to $L = \sim 100$ μm are calculated according to (2), which are denoted by $\beta_{F\text{-}P}$ and $\beta_{F\text{-}M}$, respectively and shown in Table VI. For the PMF with the same doping concentration, $\beta_{F\text{-}P}$ and $\beta_{F\text{-}M}$ is close to each other and in the energy loss rate range which is reported in [13]. The energy attenuations of I_F, which are less than 2.5×10^{-2} dB/μm for all the PMFs, are much lower than that of I_E. The highest $\beta_{F\text{-}P}$ is obtained when the concentration is 2.4 mg/g (2.34×10^{-2} dB/μm), which is consistent with the result reported in [13]. This indicates that the energy loss rate calculated by the BPNN with a well-predicted skill has a similar evaluation effect on the attenuation of the fluorescence energy.

V. CONCLUSION

In this paper, we employ the BPNN to forecast the output intensity of RhB doped PMF according to its diameter, doping concentration, and propagation distance. Through the quantitative comparison of RMSE, MAPE and R^2, the light intensity value for the PMFs with different diameters and doping concentrations can be effectively predicted by BPNN ahead of schedule, which has a good agreement with the result obtained by the traditional fitting method based on the experimental data. Besides, the energy losses of the excitation light and fluorescence from different doped PMFs are also calculated based on the predicted values. Using artificial neural networks, we could directly connect the material parameters of doped PMF to its optical properties and flexibly and conveniently acquire the energy attenuation of the PMF. This method provides a new approach to obtain the energy loss of MNF in advance and offers a valuable reference for the optimal design of MNF devices.

REFERENCES

[1] H. Q. Yu and B. J. Li, "Wavelength-converted wave-guiding in dye-doped polymer nanofibers," *Sci. Rep.*, vol. 3, no. 1, Apr. 2013, Art. no. 1674.

[2] H. Y. Li, Y. Wang, J. Li, S. Q. Liu, and J. Yang, "Waveguiding performance of rhodamine 6G doped polymer nanowire," *Optik*, vol. 127, no. 18, pp. 7268–7273, May 2016.

[3] X. Y. Li, X. Guo, D. L. Wang, and L. M. Tong, "Propagation losses in gold nanowires," *Opt. Commun.*, vol. 323, no. 15, pp. 119–122, Jul. 2014.

[4] H. G. Im *et al.*, "Flexible transparent conducting hybrid film using a surface-embedded copper nanowire network: A highly oxidation-resistant copper nanowire electrode for flexible optoelectronics," *ACS Nano*, vol. 8, no. 10, pp. 10973–10979, Oct. 2014.

[5] C. Meng, Y. Xiao, P. Wang, L. Zhang, Y. X. Liu, and L. M. Tong, "Quantum-dot-doped polymer nanofibers for optical sensing," *Adv. Mater.*, vol. 23, no. 33, pp. 3770–3774, Sep. 2011.

[6] J. H. Yu, X. B. Wang, and R. Chen, "Optical waveguiding properties of colloidal quantum dots doped polymer microfibers," *Opt. Express*, vol. 26, no. 10, pp. 13408–13415, May 2018.

[7] P. Wang, L. Zhang, Y. N. Xia, L. M. Tong, X. Xu, and Y. B. Ying, "Polymer nanofibers embedded with aligned gold nanorods: A new platform for plasmonic studies and optical sensing," *Nano Lett.*, vol. 12, no. 6, pp. 3145–3150, Jun. 2012.

[8] N. Irawati *et al.*, "Relative humidity sensing using a PMMA doped agarose gel microfiber," *J. Lightw. Technol.*, vol. 35, no. 18, pp. 3940–3944, Sep. 2017.

[9] Q. Yang, X. S. Jiang, F. X. Gu, Z. Ma, J. Y. Zhang, and L. Tong, "Polymer micro or nanofibers for optical device applications," *J. Appl. Polym. Sci.*, vol. 110, pp. 1080–1084, Oct. 2008.

[10] L. Zhang, Y. Tang, and L. M. Tong, "Micro-/nanofiber optics: Merging photonics and material science on nanoscale for advanced sensing technology," *iScience*, vol. 23, no. 1, Jan. 2020, Art. no. 100810.

[11] Y. G. Ma, X. Y. Li, H. K. Yu, L. M. Tong, Y. Gu, and Q. H. Gong, "Direct measurement of propagation losses in silver nanowires," *Opt. Lett.*, vol. 35, no. 8, pp. 1160–1162, Apr. 2010.

[12] W. H. Wang, Q. Yang, F. R. Fan, H. X. Xu, and Z. L. Wang, "Light propagation in curved silver nanowire plasmonic waveguides," *Nano Lett.*, vol. 11, no. 4, pp. 1603–1608, Apr. 2011.

[13] M. J. Li *et al.*, "Energy losses and fluorescent efficiency of RHB-doped polymer microfibers via optical waveguiding excitation," *Appl. Opt.*, vol. 59, no. 14, pp. 4542–4547, May 2020.

[14] K. W. Li, W. C. Zhou, and S. W. Zeng, "Optical micro/nanofiber-based localized plasmon resonance biosensors: Fiber diameter dependence," *Sensors*, vol. 18, no. 10, Oct. 2018, Art. no. 3295.

[15] F. X. Gu, H. K. Yu, P. Wang, Z. Y. Yang, and L. M. Tong, "Light-emitting polymer single nanofibers via waveguiding excitation," *ACS Nano*, vol. 4, no. 9, pp. 5332–5338, Sep. 2010.

[16] H. J. Sun, H. Zhang, G. Y. Feng, H. Zhou, and S. H. Zhou, "Freestanding polymeric microdisk laser based on a microfiber knot," *Laser Phys. Lett.*, vol. 14, no. 5, May 2017, Art. no. 055806.

[17] P. Das and A. Debnath, "Reactive orange 12 dye adsorption onto magnetically separable CaFe$_2$O$_4$ nanoparticles synthesized by simple chemical route: Kinetic, isotherm and neural network modeling," *Water Pract. Technol.*, vol. 16, no. 4, pp. 1141–1158, Jul. 2021.

[18] M. Bhowmik, K. Deb, A. Debnath, and B. Saha, "Mixed phase Fe$_2$O$_3$/Mn$_3$O$_4$ magnetic nanocomposite for enhanced adsorption of methyl orange dye: Neural network modeling and response surface methodology optimization," *Appl. Organometallic Chem.*, vol. 32, no. 3, Mar. 2018, Art. no. e4186.

[19] K. L. Bhowmik, A. Debnath, R. K. Nath, S. Das, K. K. Chattopadhyay, and B. Saha, "Synthesis and characterization of mixed phase manganese ferrite and hausmannite magnetic nanoparticle as potential adsorbent for methyl orange from aqueous media: Artificial neural network modeling," *J. Mol. Liquids*, vol. 219, pp. 1010–1020, Jul. 2016.

[20] A. Debnath, M. Majumder, M. Pal, N. S. Das, K. K. Chattopadhyay, and B. Saha, "Enhanced adsorption of hexavalent chromium onto magnetic calcium ferrite nanoparticles: Kinetic, isotherm, and neural network modeling," *J. Dispersion Sci. Technol.*, vol. 37, no. 12, pp. 1806–1818, Jan. 2016.

[21] N. H. Singh, K. Kezo, A. Debnath, and B. Saha, "Enhanced adsorption performance of a novel Fe-MN-Zr metal oxide nanocomposite adsorbent for anionic dyes from binary dye mix: Response surface optimization and neural network modeling," *Appl. Organometallic Chem.*, vol. 32, no. 3, Mar. 2018, Art. no. e4165.

[22] I. Suárez *et al.*, "Propagation length enhancement of surface plasmon polaritons in gold nano-/micro-waveguides by the interference with photonic modes in the surrounding active dielectrics," *J. Nanophoton.*, vol. 6, no. 5, pp. 1109–1120, Sep. 2017.

[23] K. S. Lim *et al.*, "A polyaniline-coated integrated microfiber resonator for UV detection," *IEEE Sensors J.*, vol. 13, no. 5, pp. 2020–2025, May 2013.

[24] H. M. Luo, X. W. Li, W. W. Zou, X. Li, Z. H. Hong, and J. P. Chen, "Temperature-insensitive microdisplacement sensor based on locally bent microfiber taper modal interferometer," *IEEE Photon. J.*, vol. 4, no. 3, pp. 772–778, Jun. 2012.

[25] L. M. Tong *et al.*, "Subwavelength-diameter silica wires for low-loss optical wave guiding," *Nature*, vol. 426, no. 6968, pp. 816–819, Dec. 2003.

[26] H. Zhang, M. Zhang, J. Kang, X. D. Zhang, and J. R. Yang, "High sensitivity fiber-optic strain sensor based on modified microfiber-assisted open-cavity Mach-Zehnder interferometer," *J. Lightw. Technol.*, vol. 39, no. 13, pp. 4556–4563, Jul. 2021.

[27] K. J. Lee, J. H. Oh, Y. Kim, and J. Jang, "Fabrication of Photoluminescent-dye embedded poly (methyl methacrylate) nanofibers and their fluorescence resonance energy transfer properties," *Adv. Mater.*, vol. 18, no. 17, pp. 2216–2219, Sep. 2006.

[28] Y. P. Zhang *et al.*, "Backpropagation neural network assisted concentration prediction of biconical microfiber sensors," *Opt. Express*, vol. 28, no. 25, pp. 37566–37576, Dec. 2020.

[29] D. Chicco, M. J. Warrens, and G. Jurman, "The coefficient of determination R-squared is more informative than SMAPE, MAE, MAPE, MSE and RMSE in regression analysis evaluation," *PeerJ Comput. Sci.*, vol. 7, Jul. 2021, Art. no. e623.

[30] A. de Myttenaere, B. Golden, B. L. Grand, and F. Rossi, "Mean absolute percentage error for regression models," *Neurocomputing*, vol. 192, no. 1, pp. 38–48, Jun. 2016.

[31] D. X. Liang *et al.*, "Visually adjusting coupling conditions in light-emitting micro-components," *IEEE Photon. Technol. Lett.*, vol. 31, no. 17, pp. 1425–1428, Sep. 2019.

[32] Z.-M. Huang, Y.-Z. Zhang, M. Kotaki, and S. Ramakrishna, "A review on polymer nanofibers by electrospinning and their applications in nanocomposites," *Compos. Sci. Technol.*, vol. 63, pp. 2223–2253, Nov. 2003.

[33] X. B. Xing, Y. Q. Wang, and B. J. Li, "Nanofiber drawing and nanodevice assembly in poly(trimethylene terephthalate)," *Opt. Express*, vol. 16, pp. 10815–10822, Jul. 2008.

[34] F. X. Gu *et al.*, "Large defect-induced sub-bandgap photoresponse in semiconductor nanowires via waveguiding excitation," *Nanotechnology*, vol. 22, no. 42, Oct. 2011, Art. no. 425201.